Optical properties of meteoric smoke analogues

Tasha Aylett[*1], James S. A. Brooke[1], Alexander D. James[1], Dennis Duft[2], Mario Nachbar[3], John M. C. Plane[1]*

(1) School of Chemistry, University of Leeds, Leeds, UK.

(2) Institute for Meteorology and Climate Research, Karlsruhe Institute of Technology (KIT), Karlsruhe, Germany

(3) Institute of Environmental Physics (IUP), Ruprecht-Karls-University Heidelberg, Heidelberg, Germany

Supplementary Information

Contained in this SI is the following:

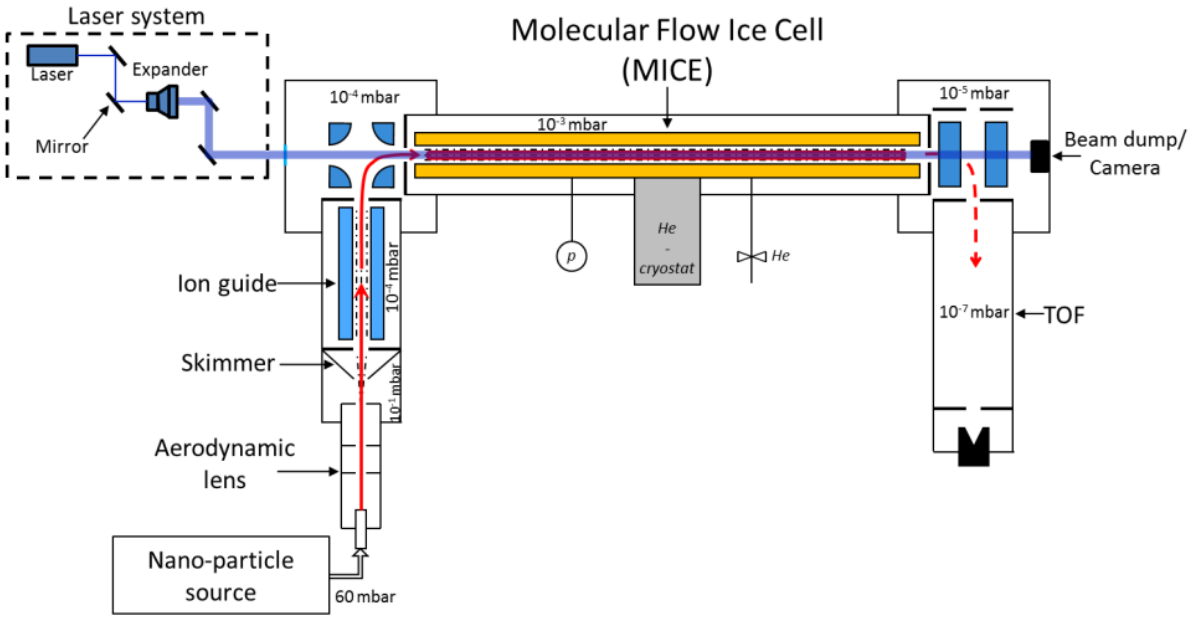

Figure S1. Schematic diagram of the TRAPS apparatus, including the MICE. Image modified from Nachbar et al. (2018).

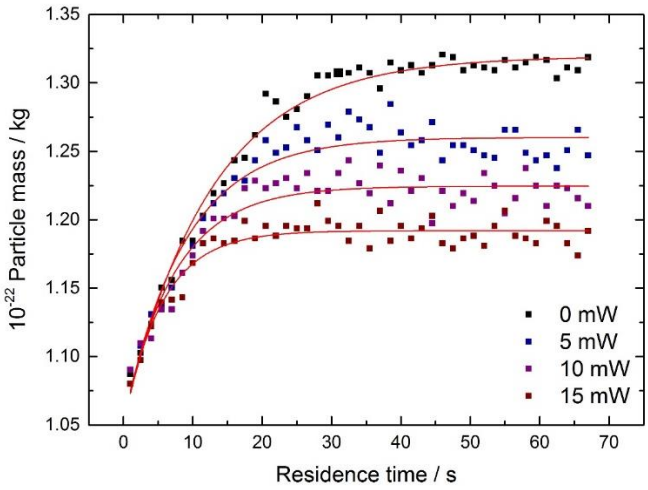

Figure S2. Average particle mass as a function of residence time in the MICE, for experimental runs under one set of conditions (supersaturation, initial particle mass)/ Irradiation of particles at 0 mW (black) 5 mW (blue) 10 mW (purple) and 15 mW (brown).

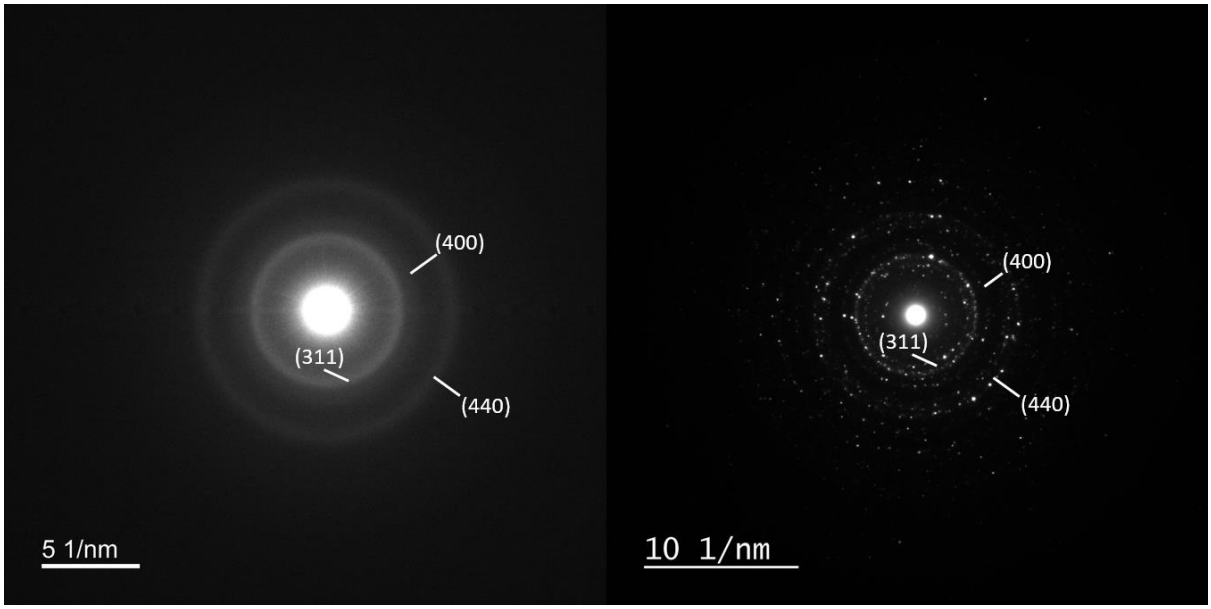

Figure S3. Left panel: TEM electron diffraction pattern of an iron oxide agglomerate, showing the intense reflections close to the 311, 400 and 440 diffraction planes. Right panel: Electron diffraction pattern for a maghemite standard.

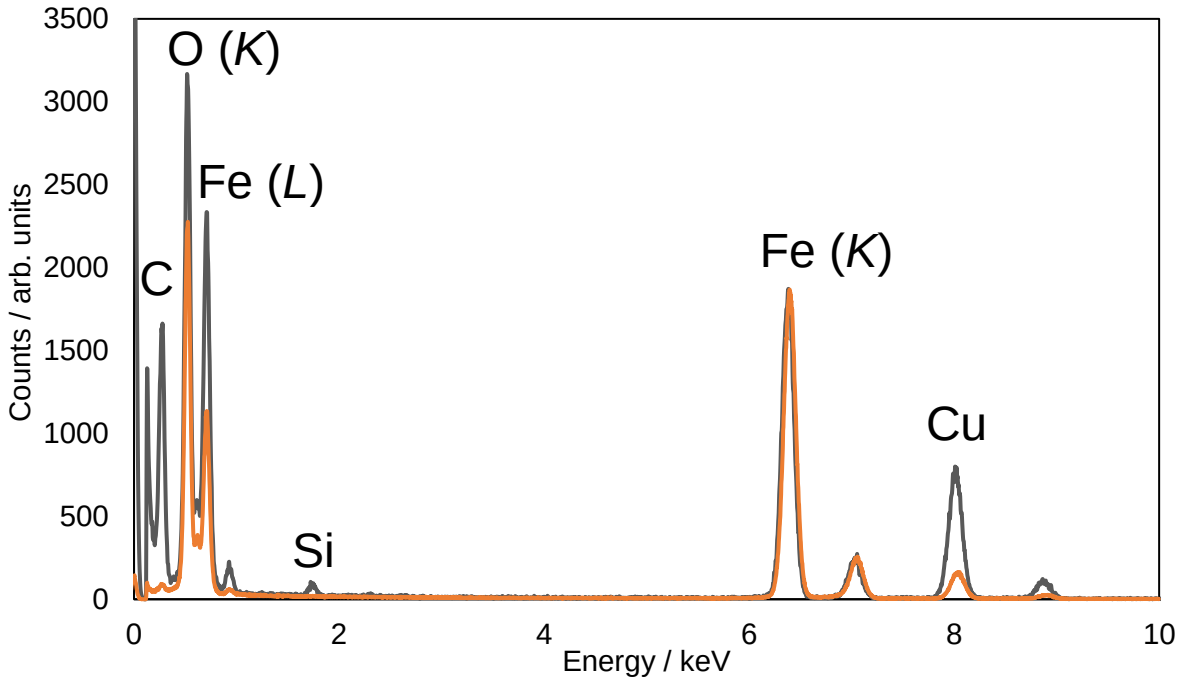

Figure S4. EDX spectrum of the iron oxide agglomerates produced in the photochemical reactor (grey) and an equivalent spectrum for a maghemite standard (orange). The spectrum for the maghemite standard has been scaled for clarity.

Table S1. Absorption cross section of $Fe(CO)_5$ at 293 K.

Wavelength /nm	Absorption Cross section / cm^2	Wavelength /nm	Absorption Cross section / cm^2
190	3.14×10^{-17}	450	1.95×10^{-20}
200	3.96×10^{-17}	460	1.76×10^{-20}
210	2.63×10^{-17}	470	1.65×10^{-20}
220	1.62×10^{-17}	480	1.57×10^{-20}
230	1.30×10^{-17}	490	1.45×10^{-20}
240	1.23×10^{-17}	500	1.39×10^{-20}
250	1.12×10^{-17}	510	1.33×10^{-20}
260	8.38×10^{-18}	520	1.29×10^{-20}
270	5.89×10^{-18}	530	1.23×10^{-20}
280	4.47×10^{-18}	540	1.18×10^{-20}
290	2.94×10^{-18}	550	1.15×10^{-20}
300	1.75×10^{-18}	560	1.09×10^{-20}
310	1.01×10^{-18}	570	1.04×10^{-20}
320	6.20×10^{-19}	580	1.01×10^{-20}
330	4.21×10^{-19}	590	9.87×10^{-21}
340	3.23×10^{-19}	600	9.40×10^{-21}
350	2.63×10^{-19}	610	9.14×10^{-21}
360	2.14×10^{-19}	620	8.69×10^{-21}
370	1.69×10^{-19}	630	8.61×10^{-21}
380	1.27×10^{-19}	640	8.42×10^{-21}
390	9.14×10^{-20}	650	7.97×10^{-21}
400	6.46×10^{-20}	660	7.96×10^{-21}
410	4.59×10^{-20}	670	7.64×10^{-21}
420	3.40×10^{-20}	680	7.30×10^{-21}
430	2.66×10^{-20}	690	7.35×10^{-21}
440	2.22×10^{-20}	700	7.07×10^{-21}

Table S2. Functions used to fit to generate imaginary refractive indices from the best-fit real refractive indices at 405, 488 and 660 nm (1-3), and the function used to define the wavelength dependence of the imaginary refractive index using values defined from best-fit data at 405, 488 and 660 nm (4).

	Wavelength / nm	Function
1	405	$y = y_0 + a_1 \cdot e^{(-x/t_1)} + a_2 \cdot e^{(-x/t_2)}$ Where $y_0 = 0.121$, $a_1 = 1 \times 10^{-29}$, $t_1 = 0.0508$, $a_2 = 0.0337$, $t_2 = 0.850$
2	488	$y = a \cdot e^{(-x/t)} + m \cdot x + c$ Where $a = 0.300$, $t = -2.73$, $m = -0.242$, $c = -0.135$
3	660	$y = a \cdot e^{(-x/t)} + m \cdot x + c$ Where $a = 0.0563$, $t = -3.10$, $m = -0.0482$, $c = -0.0220$
4	350-660	$y = a \cdot b^x$ Where $a = 238$, $b = 0.986$

References

Nachbar, M., Duft, D., Kiselev, A., and Leisner, T.: Composition, Mixing State and Water Affinity of Meteoric Smoke Analogue Nanoparticles Produced in a Non-Thermal Microwave Plasma Source, Zeit. Phys. Chem., 232, 635-648, 2018.